PAPER

Check for updates

An electrochemical sensor based on a MOF/ZnO composite for the highly sensitive detection of Cu(II) in river water samples†

Zhenshan Li,[a] Qi Li,[a] Rong Jiang,[a] Yan Qin,[a] Yan Luo,[a] Jinsong Li,[b] Wei Kong,[b] Zhiguo Yang,[b] Chao Huang,[b] Xin Qu,[b] Tao Wang,[b] Lin Cui,[a] Gang Wang, [ID] *[a] Shengchao Yang,*[ab] Zhiyong Liu [ID] *[a] and Xuhong Guo[ac]

Cu(II) ions are one of the most common forms of copper present in water and can cause bioaccumulation and toxicity in the human body; therefore, sensitive and selective detection methods are required. Herein, a copper ion sensor based on a UiO-66-NH$_2$/ZnO composite material is proposed. The UiO-66-NH$_2$/ZnO nanocomposite was prepared by an ultrasonic mixing method. The morphology and structure of the nanocomposite were studied by scanning electron microscopy (SEM), transmission electron microscopy (TEM) and X-ray diffraction (XRD). The sensitivity to Cu(II) is 6.46 μA μM^{-1} and the detection limit is 0.01435 μM. The composite material is rich in −OH and −NH$_2$ groups, which are active sites for Cu(II) adsorption. The UiO-66-NH$_2$/ZnO-modified electrode has good repeatability and anti-interference ability. The sensor was successfully used for the determination of Cu(II) in an actual water sample.

1. Introduction

Copper ions are essential trace elements in living organisms.[1] However, excessive intake of Cu(II) can cause a series of diseases such as gastrointestinal tract disorders, which poses a serious threat to human health.[2–5] It is of great significance to develop reliable and accurate strategies for the detection of copper ions. Electrochemical detection technology has attracted much attention in the field of heavy metal ion detection due to its advantages such as convenient detection, narrow detection range, fast response speed, high selectivity and high sensitivity.[6–9] Due to its high reliance on modified electrode materials, electrochemical stripping voltammetry is considered an effective strategy for the detection of heavy metal ions. The sensitivity and detection limit of heavy metal ions can be improved by pre-enrichment. In the pre-enrichment stage, the adsorption of target metal ions from the bulk solution to the surface of the working electrode is a very important process.[10–12]

Therefore, it is very important to design and synthesize modified materials with abundant adsorption sites to improve detection performance.

Metal–organic frameworks (MOFs) are a kind of crystalline porous material,[13–16] which have broad application prospects in the field of electrochemical sensing.[17,18] MOFs have the following advantages for the detection of heavy metal ions: (1) the large specific surface area and high porosity of MOFs are conducive to the adsorption of heavy metal ions on the surface of the working electrode, which effectively magnifies the signal response and improves detection sensitivity.[19] (2) The channels of MOFs with a specific shape and size endow them with good selectivity for specific analytes *via* size exclusion effects. (3) A variety of metal centers and organic ligands have different active sites, which contribute to the specific recognition of heavy metal ions. Due to these advantages, MOFs are widely used in the detection of heavy metal ions.[20,21] In recent years, the application of MOFs in heavy metal detection has attracted wide attention. Wang *et al.* synthesized a UiO-66-NH$_2$/GaOOH composite material by a simple hydrothermal method to achieve the detection of a variety of heavy ions.[22] Chen *et al.* prepared a multilayer biochar/UiO-66-NH$_2$ film by layered deposition technology, which can detect Pb(II) and Hg(II) sensitively.[23] Zou *et al.* used the hydrothermal method to prepare UiO-66-NH$_2$@MWCNT composite materials, which realized the rapid detection of cadmium ions in meat products.[24]

The enrichment of heavy metal ions on the electrode surface is an important process in the stage of heavy metal ion detection.[25] In order to improve the enrichment efficiency of heavy

[a]School of Chemistry and Chemical Engineering, Shihezi University/Key Laboratory for Green Processing of Chemical Engineering of Xinjiang Bingtuan/Key Laboratory of Materials-Oriented Chemical Engineering of Xinjiang Uygur Autonomous Region/Engineering Research Center of Materials-Oriented Chemical Engineering of Xinjiang Bingtuan, Shihezi, Xinjiang, 832003, P.R. China. E-mail: wanggang@shzu.edu.cn; shengchao.yang@shzu.edu.cn; lzyongclin@sina.com; Tel: +86-0993-2057276

[b]Tianfu Energy Co., Ltd, City Key Laboratory of Energy Conservation and Environmental Protection, Xinjiang, 832000, China

[c]State Key Laboratory of Chemical Engineering, East China University of Science and Technology, Shanghai 200237, P. R. China

† Electronic supplementary information (ESI) available. See DOI: 10.1039/d1ra08376g

metal ions, composite materials with different adsorption groups were designed to effectively enrich heavy metal ions on the electrode surface, and realize the purpose of highly sensitive detection of heavy metal ions. Based on its large specific surface area, excellent water stability and chemical stability,[26] UiO-66-NH$_2$ of the MOF family can be used as an excellent electrode modified material. UiO-66-NH$_2$ contains abundant amino groups,[27] which can provide active centers for the adsorption of heavy metal ions. In recent years, metal oxides have been widely used in the field of electrochemistry.[28–30] ZnO has also been widely used in the field of detecting heavy metals. Orawon Chailapakul *et al.* used the colloidal coagulation effect to prepare ZnO@G nanocomposites by a simple room temperature method, which can simultaneously detect Cd(II) and Pb(II) in actual wastewater samples.[31] Thambidurai *et al.* synthesized cobalt-doped zinc oxide/reduced graphene oxide (Co:ZnO/RGO) nanorods by a chemical co-precipitation method for the electrochemical detection of Cd(II) and Pb(II).[32] The composite has excellent sensitivity for Cd(II) and Pb(II). Liu *et al.* prepared ZnO nanofibers by electrospinning and used Nafion as a binder to prepare a ZnO NF-modified glass carbon electrode for the determination of Cd(II) in water samples.[33] ZnO can be used as an adsorbent[34,35] and a detection material for heavy metal ions because of its low toxicity, excellent stability[33] and many hydroxyl groups on the nano-ZnO. These groups can capture metal ions and make heavy metal ions easily adsorbed onto the ZnO surface *via* coordination.[36] Since –NH$_2$ and –OH groups are both electron-donating groups, they coordinate with Cu(II) *via* Lewis interaction, and then can chelate and adsorb Cu(II).[35–38] Therefore, the combination of UiO-66-NH$_2$ and nano zinc oxide may enhance the perception of heavy metals. The synergistic effect of ZnO and UiO-66-NH$_2$ enhances the enrichment of target metal ions on the electrode surface, and promotes the trace detection of Cu(II) ultimately.

In this work, a novel and simple electrochemical strategy is proposed, and we prepared an electrode modified by a UiO-66-NH$_2$/ZnO composite material. The metal–organic framework and the metal oxide were successfully combined and used for the electrochemical detection of copper ions (Scheme 1). The composite material is rich in –OH and NH$_2$ groups, which can be used as active sites for Cu(II) adsorption. The surface morphology and structure of the UiO-66-NH$_2$/ZnO material were characterized by scanning electron microscopy (SEM) and X-ray photoelectron spectroscopy (XPS). Experimental parameters such as zinc oxide dosage and supporting electrolyte were optimized. The sensitivity of the UiO-66-NH$_2$/ZnO composite electrode to Cu(II) is as high as 6.46 μA μM^{-1}, and the detection limit is as low as 0.01435 μM. The composite material contains abundant active sites such as –OH and –NH$_2$ groups for Cu(II) adsorption and demonstrates excellent detection performance. In addition, the repeatability and anti-interference ability of Cu(II) detection with a modified electrode were studied, and the modified electrode was used to detect Cu(II) in actual river water.

2. Experiment

2.1. Materials

Hexamethylenetetramine (HMT), 2-aminoterephthalic acid (NH$_2$-H$_2$BDC, >98%), zinc nitrate hexahydrate (Zn(NO$_3$)$_2$·6H$_2$O) and zirconium chloride (ZrCl$_4$, ≥99.9%) were purchased from Aladdin. Anhydrous ethanol, *N,N*-dimethylformamide (DMF) and acetic acid were purchased from Fuyu Chemical Co., Ltd. (Tianjin). Copper nitrate (Cu(NO$_3$)$_2$) was purchased from Shanghai Macklin Biochemical Technology Co., Ltd. (China). Carbon cloth (hydrophilic carbon cloth, specification: 220 g) was purchased from Shanghai Lishuo Composite Material Technology Co., Ltd. Acetate buffer solution (HAc-NaAc solution, pH 5.0, 0.1 M) was prepared by mixing 15 mL acetic acid with 35 mL sodium acetate.[39] All reagents are analytically pure and can be used directly without further purification.

2.2. Apparatus

Transmission electron microscopy (Tecnai G2F20, USA), field emission scanning electron microscopy (SU8020, Japan), X-ray diffraction (D8, Bruker, Germany) and X-ray photoelectron spectroscopy (Thermo ESCALAB 250xi, Thermo Fisher, USA) were performed to analyse the morphology and structure of the material. All electrochemical tests were performed using a CHI 760E Chenhua Electrochemical Workstation (Shanghai, China). A three-electrode system was used, in which a glassy carbon electrode with a diameter of 3 mm was used as the working electrode, a Ag/AgCl electrode as the reference electrode, and a Pt wire as the counter electrode.

2.3. Preparation of ZnO

ZnO was prepared by electrochemical deposition.[40,41] The carbon cloth was ultrasonically cleaned with acetone, ethanol and deionized water in sequence for 30 minutes and then dried. With 5 mmol L^{-1} HMT and 5 mmol L^{-1} Zn(NO$_3$)$_2$·6H$_2$O as electrolytes, the carbon cloth (7 cm × 5 cm) used as a substrate was immersed into the three-electrode system and connected with the working electrode. After the reaction was completed, the product was washed with deionized water and separated from the carbon cloth, and finally, the sample was dried at 60 °C.

2.4. Preparation of UiO-66-NH$_2$

UiO-66-NH$_2$ was successfully synthesized by a slightly modified hydrothermal synthesis method.[16] First, 1 mmol 2-aminoterephthalic acid and 1 mmol ZrCl$_4$ were dissolved in a DMF (50 mL) solution under stirring, and then a certain amount of acetic acid was added to this solution and sonicated for 30 minutes. The mixed solution was moved to a 100 mL polytetrafluoroethylene-lined stainless steel autoclave. The reaction temperature was 120 °C and the reaction time was 24 h. After the reaction was completed, the reaction kettle was cooled to room temperature naturally, and the product was centrifuged
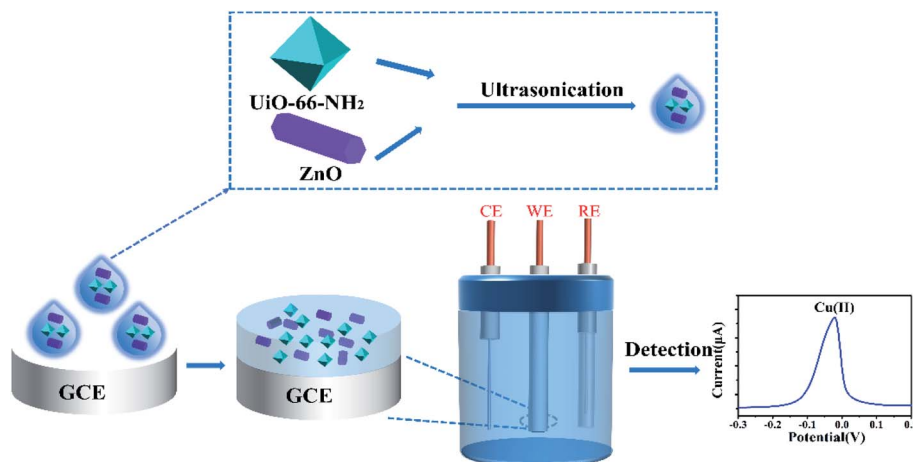
Scheme 1 Schematic diagram of the preparation of the UiO-66-NH$_2$/ZnO composite material and the electrochemical detection of copper ions.

and washed several times with DMF and anhydrous ethanol, followed by vacuum drying for 12 h to obtain UiO-66-NH$_2$.

2.5. Preparation of UiO-66-NH$_2$/ZnO composites

UiO-66-NH$_2$/ZnO composites were prepared by an ultrasonic method. Under magnetic stirring, 60 mg UiO-66-NH$_2$ was added into 2.5 mL anhydrous ethanol and stirred for 30 min to form UiO-66-NH$_2$ dispersion. At the same time, x mg ZnO ($x = 20, 40, 60, 80, 100$) was dispersed in 2.5 mL anhydrous ethanol and stirred for 30 min to form different amounts of ZnO dispersions. The UiO-66-NH$_2$ dispersion was mixed with the ZnO dispersion, and the mixture was sonicated for 1 h, followed by vacuum drying at 60 °C for 12 h to obtain UiO-66-NH$_2$/ZnO products with different mass ratios (U : Z = 3 : 1, 3 : 2, 3 : 3, 3 : 4, and 3 : 5; U : Z stands for UiO-66-NH$_2$: ZnO).

2.6. Preparation of modified electrodes

The electrode surface was polished with 1 μm, 0.3 μm and 0.05 μm Al$_2$O$_3$ powder respectively, and then the electrode was ultrasonically cleaned with anhydrous ethanol and deionized water. First, 2 mg UiO-66-NH$_2$/ZnO sample was dispersed into the ethanol–Nafion mixed solution (volume ratio 9 : 1), and the stable suspension was formed by ultrasonic treatment for 20 min. Then, 5 μL dispersion was added to the surface of the glassy carbon electrode and dried naturally to obtain a UiO-66-NH$_2$/ZnO-modified GCE. UiO-66-NH$_2$ and ZnO modified electrodes were also prepared for a comparative study. The same preparation method as UiO-66-NH$_2$/ZnO/GCE was also used to prepare UiO-66-NH$_2$ and ZnO-modified electrodes. The modified electrodes obtained are denoted as UiO-66-NH$_2$/GCE and ZnO/GCE, respectively.

2.7. Electrochemical measurements

Under the optimized experimental conditions, a HAc-NaAc solution (0.1 M, pH 5.0) was used as the supporting electrolyte, and different concentrations of Cu(ii) ions were added.

Differential pulse stripping voltammetry (DPSV) was used for electrochemical measurement. The deposition potential was −1.2 V, and the deposition time was 120 s.

3. Results and discussion

3.1. Characterization of materials

The morphology, structure and composition of synthetic materials were characterized by SEM, TEM, XRD and XPS. It can be seen from the SEM and TEM images of UiO-66-NH$_2$ (Fig. 1a and d) that the morphology of UiO-66-NH$_2$ prepared by a hydrothermal synthesis method was regular and presented a uniform octahedral structure with a size of about 50–200 nm.[23] SEM and TEM images of ZnO (Fig. 1b and e) show that ZnO nanorods have a nanorod structure with an average diameter of 250 nm and a hexagonal wurtzite crystal structure.[41] As can be seen from SEM and TEM images in Fig. 1c and f, UiO-66-NH$_2$/ZnO composites prepared by an ultrasonic mixing method are evenly dispersed with each other.

The XRD spectra of ZnO, UiO-66-NH$_2$ and UiO-66-NH$_2$/ZnO are shown in Fig. 2. The characteristic diffraction peaks of the prepared UiO-66-NH$_2$ are in good agreement with the characteristic peak of simulated UiO-66-NH$_2$, and the clear characteristic peaks indicate that the crystallinity is good.[42,43] It is proved that the crystal framework of UiO-66-NH$_2$ was successfully prepared. The XRD pattern of ZnO has obvious characteristic diffraction peaks at 31.8° (100), 34.4° (002), 36.3° (101), 47.6° (102), 56.7° (110), 62.9° (103), 66.4° (200), 68.0° (112), and 69.1° (201), which are consistent with the typical ZnO wurtzite structure (PDF#79-0206). The sharp diffraction peaks indicate that the prepared ZnO has high crystallinity. The XRD spectra of UiO-66-NH$_2$/ZnO not only show the characteristic peak of UiO-66-NH$_2$, but also show the characteristic peak of ZnO. It indicates that the main skeleton structure of UiO-66-NH$_2$ remains intact during the preparation process, which also indicates that the composite material was successfully prepared.

Fig. 3 shows the XPS spectra of UiO-66-NH$_2$ and UiO-66-NH$_2$/ZnO. In Fig. 3a, the characteristic peaks of C 1s, O 1s, N 1s and
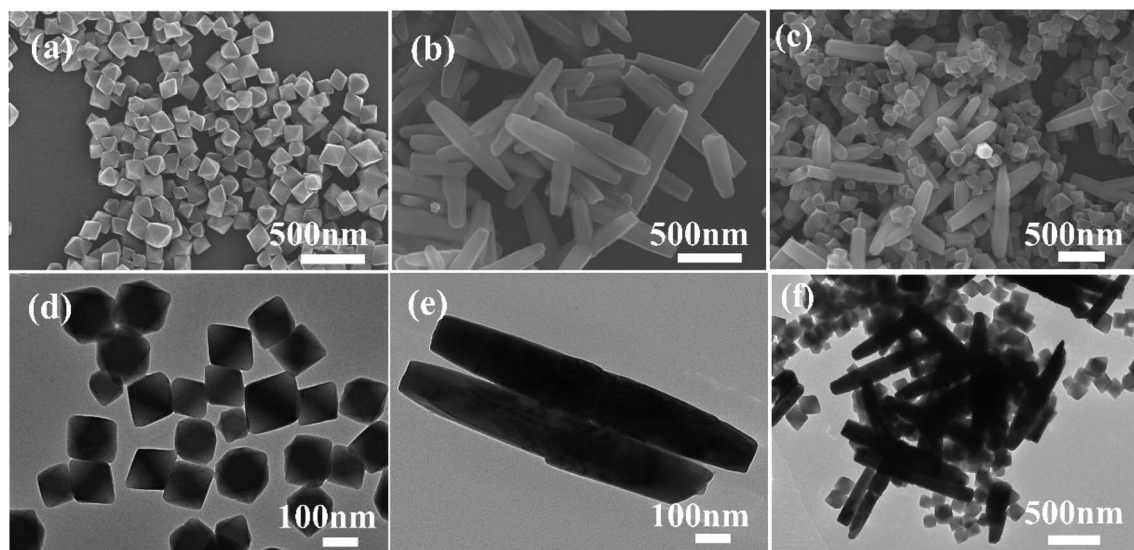
Fig. 1 SEM images of (a) UiO-66-NH$_2$, (b) ZnO, and (c) UiO-66-NH$_2$/ZnO, and TEM images of (d) UiO-66-NH$_2$, (e) ZnO, and (f) UiO-66-NH$_2$/ZnO.

Zr 3d appear in the full spectrum of UiO-66-NH$_2$. For UiO-66-NH$_2$/ZnO, in addition to the characteristic peaks of the above-mentioned elements, a group of characteristic peaks of Zn 2p also appeared, which proves that ZnO successfully modified UiO-66-NH$_2$. In order to further analyze the state of each element, the high-resolution spectra of each element were studied. The C 1s core level spectra are shown in Fig. 3b. A binding energy of 284.6 eV was obtained in the XPS analysis standardized for specimen charging using C 1s as the reference. The high-resolution spectrum of C 1s of UiO-66-NH$_2$ shows three peaks at 284.6 eV, 285.6 eV and 288.6 eV, corresponding to C–C&C–H, C–N, and O–C=O, respectively.[20,44] The binding energy of the UiO-66-NH$_2$/ZnO composite has little change before and after functionalization, which indicates that the addition of ZnO has no obvious effect on the C atom. Fig. 3c

shows the N 1s spectra of UiO-66-NH$_2$ and UiO-66-NH$_2$/ZnO. The peaks at 399.4 eV and 401.1 eV are attributed to –NH$_2$ and –NH$_3^+$ (the interaction between amino group and proton).[27] The binding energy of the composite has little change before and after functionalization, which indicates that the UiO-66-NH$_2$/ZnO composite has no obvious effect on the N atom. Fig. 3d shows the O 1s spectra of UiO-66-NH$_2$ and UiO-66-NH$_2$/ZnO.

The peak at 531.7 eV is attributed to Zr–O.[20,23] Compared with UiO-66-NH$_2$, the O 1s spectrum of composite material has a significant change. The deconvoluted O 1s peak consists of three peaks. In addition to Zr–O (531.2 eV), there also appeared Zn–O (530.3 eV) and O–H[45] (532.0 eV), which proved the successful preparation of the UiO-66-NH$_2$/ZnO composite. By comparison, the Zr–O binding energy of the composite has no obvious change except that it shifted by 0.5 eV toward a lower energy. In addition, the Zr 3d spectra of UiO-66-NH$_2$ can be deconvoluted into two distinct peaks (Fig. 3e), and the peaks at 182.8 eV and 185.1 eV are attributed to Zr 3d$_{5/2}$ and Zr 3d$_{3/2}$, respectively.[44] The binding energy of the UiO-66-NH$_2$/ZnO composite has little change before and after functionalization, which indicates that the addition of ZnO has no obvious effect on Zr atoms.

The N$_2$ adsorption–desorption isotherm and pore size distribution of UiO-66-NH$_2$, ZnO and UiO-66-NH$_2$/ZnO are shown in Fig. S1.† In Fig. S1(a),† the nitrogen adsorption–desorption isotherm of UiO-66-NH$_2$ and UiO-66-NH$_2$/ZnO has a typical type I curve, which confirms the typical microporous structure.[44] BET surface areas and pore volumes are presented in Table S1.† The BET surface area and total pore volume of UiO-66-NH$_2$ are 933.2075 m^2 g^{-1} and 0.6914 cm^3 g^{-1}, respectively; this result proves that UiO-66-NH$_2$ has a large specific surface area.[23] The BET surface area of UiO-66-NH$_2$/ZnO is 433.4271 m^2 g^{-1}, which is lower than that of UiO-66-NH$_2$.
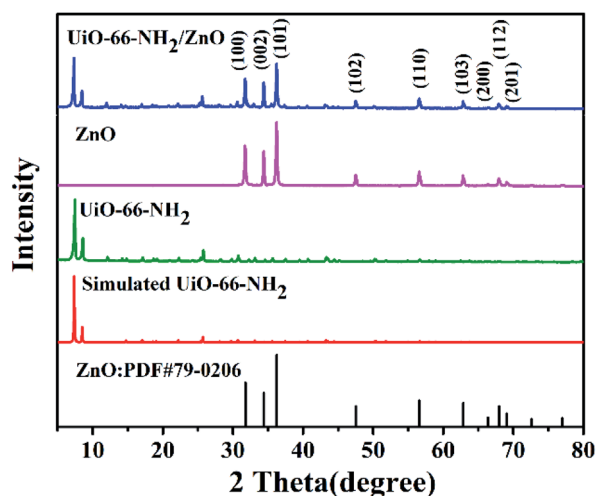

Fig. 2 XRD patterns of the standard card for ZnO, simulated UiO-66-NH$_2$, prepared UiO-66-NH$_2$, prepared ZnO, and UiO-66-NH$_2$/ZnO.
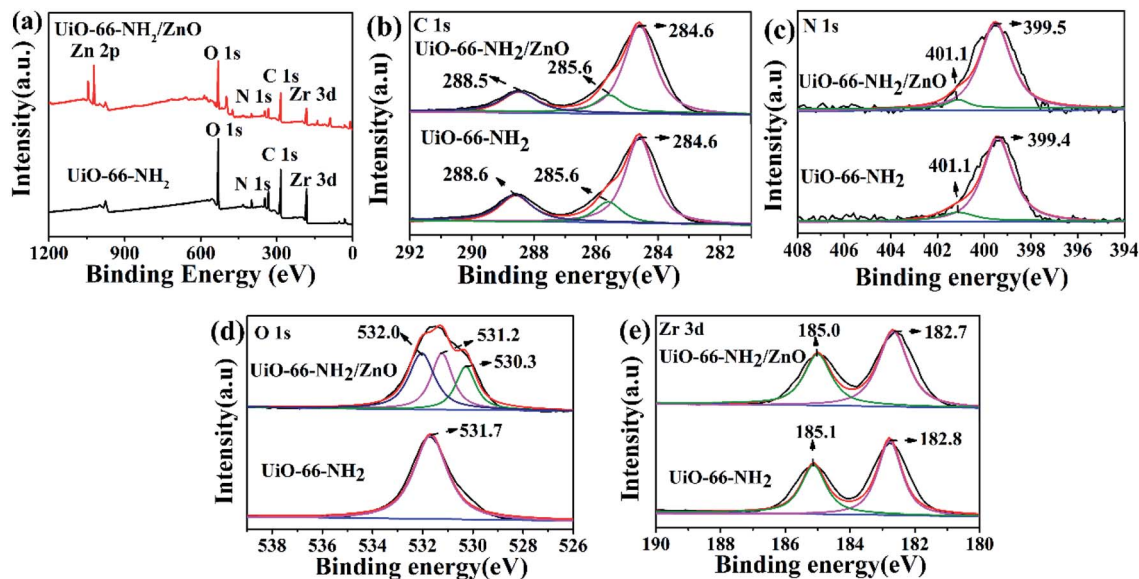
Fig. 3 XPS spectra of the UiO-66-NH$_2$ and UiO-66-NH$_2$/ZnO: (a) full-scan spectrum, (b) C 1s, (c) N 1s, (d) O1s, (e) Zr 3d.

3.2. Electrochemical experimental characterization

The electrochemical behaviors of bare GCE, UiO-66-NH$_2$, UiO-66-NH$_2$/ZnO and ZnO-modified electrodes were investigated by cyclic voltammetry (CV). The CV tests were carried out in a 0.1 M HAc-NaAc solution (pH = 5.0) containing 3.0 μM Cu(II) at a voltage range of −0.4 V to 0.4 V at a scanning rate of 0.1 V s^{-1}. Fig. 4a shows the CV curves for the electrochemical detection of Cu(II) by the four above-mentioned modified electrode materials. Compared with the bare GCE, UiO-66-NH$_2$/GCE, ZnO/GCE and UiO-66-NH$_2$/ZnO/GCE all have a pair of redox peaks, while UiO-66-NH$_2$/ZnO/GCE shows more obvious redox peaks.

The mass transfer process of the modified electrodes was studied by recording the CV curves on bare GCE, UiO-66-NH$_2$/GCE, ZnO/GCE and UiO-66-NH$_2$/ZnO/GCE with different scan rates in a 0.1 M HAc-NaAc solution (pH = 5.0) containing 3.0 μM Cu(II), as shown in Fig. 4b and S2.† When the scanning rate increases from 10 mV s^{-1} to 100 mV s^{-1}, the anode peak current of UiO-66-NH$_2$/ZnO/GCE increases gradually and the current has a linear relationship with the square root of the scanning

rate (Fig. 4c): $I_{pa} = 5.47V^{1/2} + 1.11$ ($R^2 = 0.962$), indicating that the diffusion-controlled mass transfer process occurs on the GCE modified by UiO-66-NH$_2$/ZnO.[46,47] The R^2 values of other three modified electrodes are 0.996 (bareGCE), 0.986 (UiO-66-NH$_2$/GCE) and 0.996 (ZnO/GCE), which are also the diffusion-controlled process. This indicates that Cu(II) has better absorption and diffusion on the UiO-66-NH$_2$/ZnO/GCE surface, which is beneficial for electrochemical sensing towards Cu(II).

3.3. Optimization of the experimental parameters

In order to optimize the detection performance of the UiO-66-NH$_2$/ZnO-modified electrode, the experimental parameters such as mass ratios of UiO-66-NH$_2$ and ZnO, supporting electrolytes, pH values, enrichment potential and enrichment time were optimized. The ratio of UiO-66-NH$_2$ and ZnO in the UiO-66-NH$_2$/ZnO composite will affect the detection performance of the electrode, and an appropriate ratio will improve the detection performance.[48] The supporting electrolyte plays a buffer role in the detection process of Cu(II).[49] The pH value of the solution is
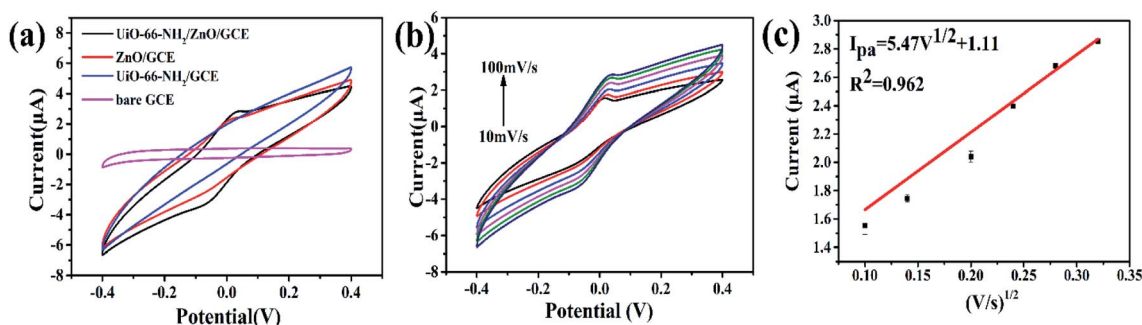

Fig. 4 (a) CV curves of 3.0 μM Cu(II) for different electrodes at a scan rate of 100 mV s^{-1} in 0.1 M HAc–NaAc buffer solution (pH = 5.0). (b) CV curves of 3.0 μM Cu(II) for UiO-66-NH$_2$/ZnO/GCE in 0.1 M HAc–NaAc solution (pH = 5.0) at different scan rates: 10–100 mV s^{-1}. (c) Plots of the linear relationship between the anodic peak current (I_{pa}) and the square root of scan ($V^{1/2}$) of UiO-66-NH$_2$/ZnO/GCE.

one of the important parameters that affect the adsorption process of metal ions on the electrode material, because metal ions will undergo hydrolysis reactions under alkaline conditions.[27] The deposition potential may lead to unwanted dissolution or oxide formation on the electrode surface, so it must be optimized.[48] The deposition time will affect the amount of metal ions accumulated on the electrode surface. Therefore, it can affect the peak current of the detected ions.[50]

The current peak values of 2 μM Cu(II) with different mass ratios of UiO-66-NH$_2$ and ZnO were compared. As shown in Fig. 5a, the current response of the modified electrode toward Cu(II) increases with the increase in U : Z from 3 : 1 to 3 : 3, and reaches its maximum at 3 : 3 (U : Z stands for UiO-66-NH$_2$: ZnO). However, with the continuous increase in U : Z ratio, the peak current presents a downward trend. This may be due to the fact that in the range of U : Z ratio 3 : 1–3 : 3, hydroxyl active sites on the ZnO increased with the increase in ZnO content, and more Cu(II) can be enriched to reach the electrode surface. However, when the content of ZnO is too high, it may occupy part of the –NH$_2$ active site of UiO-66-NH$_2$, making the peak current decrease instead. Therefore, U : Z = 3 : 3 was selected as the optimal ratio of the composite material.

The supporting electrolyte has a great impact on the electrochemical detection of heavy metal ions. Because the supporting electrolyte has the ability to fix pH and ionic strength, it can play a buffering role in the detection of metal ions.[51]

Fig. 5b shows the current response toward 2 μM Cu(II) in phosphate buffered saline (PBS) and HAc-NaAc electrolyte solutions (0.1 M, pH = 5.0). It can be seen that when HAc-NaAc is used as an electrolyte solution, the peak current for Cu(II) is larger. This may be because the ionic strength of the PBS buffer is less than that of the HAc-NaAc buffer, and its buffering effect

is poor.[49] While the HAc-NaAc buffer has the least competition for ion exchange centers on the electrode surface, it is suitable as a supporting electrolyte solution.[48,52] Therefore, the HAc-NaAc solution was used as the electrolyte. The influence of the pH value on the peak current was further investigated. As shown in Fig. 5c, the peak current increases as the pH value increases from 4.0 to 5.0 and reaches its maximum value at a pH value of 5.0. As the pH value further increases, the peak current gradually decreases. This may be due to the fact that the amino and hydroxyl groups of the UiO-66-NH$_2$/ZnO composite are easy to be protonated at a low pH value,[53] which is not conducive to the adsorption of Cu(II) onto the modified material. Conversely, when the pH value is greater than 5.0, the decrease in peak current may be related to the hydrolysis of Cu(II) to form metal hydroxides.[27,54] Therefore, 5.0 was selected as the best pH value for subsequent experiments.

Since deposition potential and deposition time have great influence on Cu(II) stripping current, the electrochemical response of different deposition potentials and deposition times toward Cu(II) was further studied. The range of deposition potential was set to be from −1.0 V to −1.4 V (Fig. 5d). The peak current increases as the deposition potential increases from −1.0 V to −1.2 V, and reaches its maximum value at −1.2 V. Because the negative shift of the deposition potential promotes the reduction of Cu(II) on the electrode surface.[20] However, when the deposition potential changes from −1.2 to −1.4 V, the peak current decreases accordingly; this may be because the excessively negative deposition potential causes hydrogen evolution reactions on the electrode surface, which prevents the deposition of metal ions on the electrode surface;[48,50,55] therefore, −1.2 V was selected as the optimal deposition potential. The optimized results of deposition time are shown in Fig. 5e.
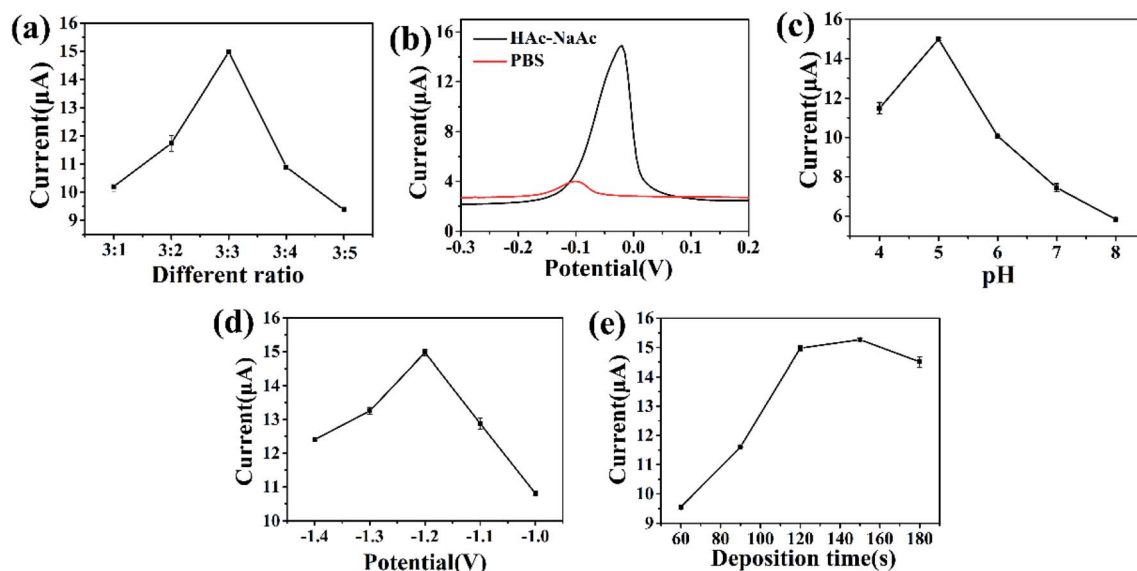

Fig. 5 (a) Peak current comparison of 2.0 μM Cu(II) for the UiO-66-NH$_2$/ZnO composite modified electrode with different concentration ratios (U : Z = 3 : 1–3 : 5, U : Z stands for UiO-66-NH$_2$: ZnO) in 0.1 M HAc-NaAc solution (pH = 5.0). Influence of various experimental parameters on the DPSV response of UiO-66-NH$_2$/ZnO/GCE toward Cu(II) (2 μM): (b) supporting electrolytes; (c) pH; (d) deposition potential; and (e) deposition time.
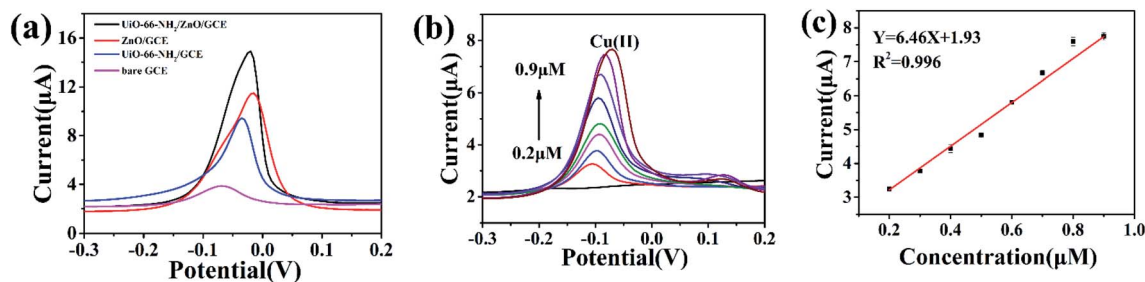
Fig. 6 (a) DPSV curves of 2.0 μM Cu(II) for different electrodes in 0.1 M HAc-NaAc solution (pH = 5.0). (b) DPSV responses of the UiO-66-NH$_2$/ZnO modified electrodes toward Cu(II) at different concentrations in 0.1 M HAc-NaAc solution (pH = 5.0). (c) Plots of linear relationship between the peak current and the concentration of Cu(II) of UiO-66-NH$_2$/ZnO/GCE.

The deposition time range is set as 60–180 s. With the increase in deposition time from 60 s to 180 s, the corresponding peak current toward Cu(II) increases obviously. When the deposition time exceeds 120 s, the peak current basically remains unchanged. This may be related to the adsorption saturation of Cu(II) on the electrode surface.[56] Therefore, 120 s was selected as the best deposition time.

3.4. Analytical performance for Cu(II)

For the sake of evaluation of the detection performance of modified electrodes, the electrochemical responses of different modified electrodes were studied in 2.00 μM Cu(II) solution under optimal experimental conditions. As shown in Fig. 6a, the bare GCE showed a weak dissolution peak current. When the electrode was modified with UiO-66-NH$_2$, the dissolution peak current significantly increased. Compared with the bare GCE and UiO-66-NH$_2$/GCE, the dissolution peak current toward Cu(II) was significantly increased by UiO-66-NH$_2$/ZnO/GCE. This indicates that the UiO-66-NH$_2$/ZnO composite has excellent detection performance toward Cu(II). The reasons are as follows: (1) due to the large specific surface area and polyhedral structure of UiO-66-NH$_2$, the active site is fully exposed, which promotes the adsorption and enrichment of Cu(II) on the electrode surface[27] and (2) UiO-66-NH$_2$/ZnO composites provide abundant –OH[57] and –NH$_2$ groups, which can be used as active sites for Cu(II) adsorption.

Under the optimized experimental conditions, UiO-66-NH$_2$/ZnO/GCE was used to detect Cu(II) of different concentrations. As shown in Fig. 6b, the peak current increases linearly with the increase in Cu(II) concentration in the range of 0.2–0.9 μM. As shown in Fig. 6c, the linear regression equation was $Y = 6.46X + 1.93$ ($R^2 = 0.996$), the sensitivity was 6.46 μA μM^{-1}, and the

detection limit (S/N = 3) was as low as 0.01435 μM. In this paper, the UiO-66-NH$_2$/ZnO/GCE was compared with other reported Cu(II) electrochemical sensors, as shown in Table 1.[18,21,22,50,58] The results indicate that the UiO-66-NH$_2$/ZnO-modified electrode has better sensitivity for Cu(II).

3.5. Repeatability and interference study

As shown in Fig. 7a, the repeatability of UiO-66-NH$_2$/ZnO/GCE was studied by measuring 13 times at the same modified electrode in 2 μM Cu(II) solution and recording the current response each time. It can be seen from the figure that the peak current of 13 times has little change. The relative standard deviation (RSD) is 1.55%, indicating that the UiO-66-NH$_2$/ZnO/GCE electrode has good electrochemical detection stability. In order to study the anti-interference ability of UiO-66-NH$_2$/ZnO/GCE, common interfering ions were added into 0.8 μM Cu(II) solution. As shown in Fig. 7b, when interfering ions (Mg(II), Li(I), Na(I), K(I), and Ca(II)) were added, the peak current of Cu(II) ions did not change significantly (the concentration of interfering ions is 10 times that of Cu(II)); even after the mixture of all ions was added, the peak current of Cu(II) did not change significantly. As shown in Table 2, in the presence of interfering ions, the relative deviation of the peak current of Cu(II) is less than ±2%, indicating that these interfering ions have a little influence on the electrochemical detection of Cu(II). UiO-66-NH$_2$/ZnO has good anti-interference performance.

3.6. Real sample analysis

In order to evaluate the practical application of the prepared UiO-66-NH$_2$/ZnO/GCE, Cu(II) in the real water sample of Mahe

Table 1 Comparison of various electrode materials for the determination of Cu(II)

Electrodes	Detection limit (μM)	Sensitivity (μA μM^{-1})	Electrolyte	Ref.
MIL-101 (Cr)	0.011	—	0.2 M HAc-NaAc (pH 5.2)	18
ZIF-67/MWCNT/Nafion	0.001	—	0.1 M HAc-NaAc (pH 2.0)	21
UiO-66-NH$_2$/GaOOH	0.026	1.878	0.1 M PBS (pH 6.0)	22
GA-UiO-66-NH$_2$/GCE	0.007	0.7314	0.2 M HAc-NaAc (pH 5.0)	50
PA/PPy/ZIF-8@ZIF-67	0.0148	0.169	0.1 M HAc-NaAc (pH 4.5)	58
UiO-66-NH$_2$/ZnO	0.01435	6.46	0.1 M HAc-NaAc (pH 5.0)	This work

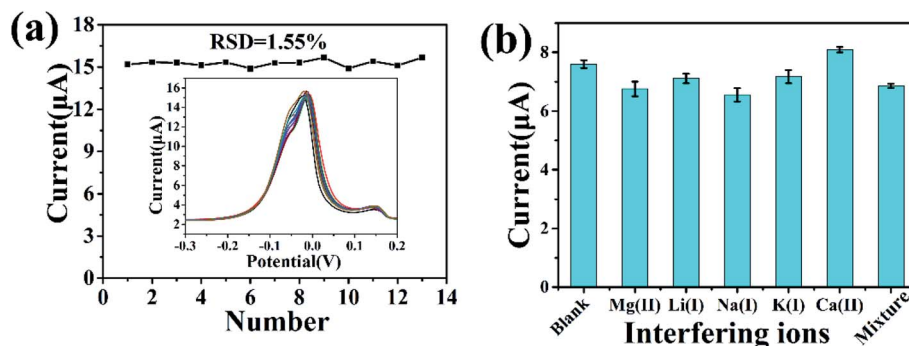**Fig. 7** Repeatability (a) measurements of the DPSV response for 2.0 μM Cu(ɪɪ) on UiO-66-NH$_2$/ZnO/GCE in 0.1 M HAc-NaAc solution (pH = 5.0). (b) Interference studies of UiO-66-NH$_2$/ZnO in 0.1 M HAc-NaAc solution (pH = 5.0) containing 0.8 μM Cu(ɪɪ); the concentration of each interfering ion is 8 μM, which is 10-fold that of the target metal ions.

Table 2 Interference of other metal ions on the peak current of Cu(ɪɪ)

Interfering ions	Concentration (μM)	Signal change (%)
Mg(ɪɪ)	8	−0.11
Li(ɪ)	8	−0.06
Na(ɪ)	8	−0.14
K(ɪ)	8	−0.05
Ca(ɪɪ)	8	0.06
Mixture	8	−0.10

Table 3 Determination of Cu(ɪɪ) in real samples and its spiked recovery

Samples	Spiked (μM)	Found (μM)	Recovery (%)	RSD ($n = 3$) (%)
Sample 1	0.5	0.490	98.0	2.1
Sample 2	0.6	0.563	93.8	2.0
Sample 3	0.7	0.684	97.7	1.8

modified electrode shows a good application potential in practical water samples.

Reservoir in Shihezi, Xinjiang, China was detected. Before the experiment, the impurities in the real water sample were filtered through a filter membrane and diluted with 0.1 M HAc-NaAc buffer (pH = 5.0) at a 9 : 1 volume ratio. Then, it was used for the electrochemical detection and analysis, as shown in Fig. 8a. It is worth noting that a weak dissolution peak of Cu(ɪɪ) can still be observed without adding any concentration of Cu(ɪɪ) (Fig. 8b), indicating that trace amounts of Cu(ɪɪ) are present in the real water sample. When different concentrations of Cu(ɪɪ) were added, the peak current increased gradually. As shown in Table 3, the average recovery ranged from 97.7% to 98%. As shown in Fig. 8c, the sensitivity was slightly reduced compared with the Cu(ɪɪ) detection (6.46 μA μM^{-1}) in deionized water, which may be due to more interference factors in the real water sample. In conclusion, the satisfactory recovery of the UiO-66-NH$_2$/ZnO-

Conclusions

In summary, a UiO-66-NH$_2$/ZnO composite has been successfully prepared and used for the determination of Cu(ɪɪ). Under the optimized experimental conditions, the detection limit of the UiO-66-NH$_2$/ZnO-modified electrode for Cu(ɪɪ) is 0.01435 μM. This could be attributed to the polyhedral structure and large specific surface area of UiO-66-NH$_2$, which fully exposes the active site, and the abundant –OH and –NH$_2$ groups in the composite material can be used as the active site for Cu(ɪɪ) adsorption. In addition, UiO-66-NH$_2$/ZnO/GCE has good repeatability and anti-interference ability, which can be used for the detection of Cu(ɪɪ) in actual water samples. These results indicate that the synthesized UiO-66-NH$_2$/ZnO composite has a broad application prospect in the field of Cu(ɪɪ) detection.
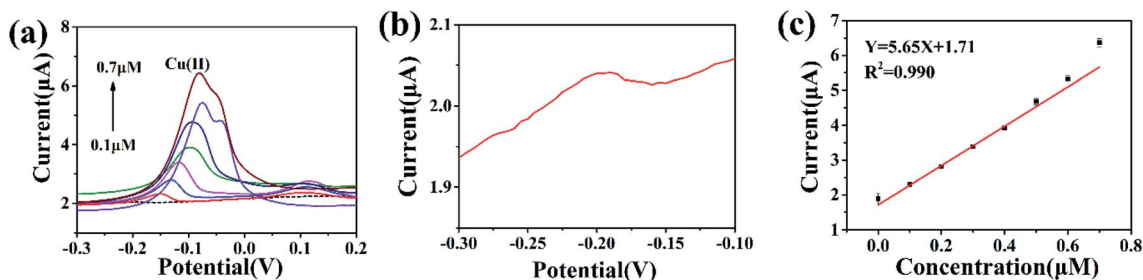

Fig. 8 (a) Detection of Cu(ɪɪ) in real water samples by adding different concentrations of Cu(ɪɪ) to UiO-66-NH$_2$/ZnO/GCE. (b) Blank value when copper is not added to the real water sample. (c) Calibration curve between stripping peak current and Cu(ɪɪ) concentration.

Conflicts of interest

The authors declare that they have no known competing financial interests or personal relationships that could have appeared to influence the work reported in this paper.

Acknowledgements

References

1 N. Wang, H. Dai, D. Wang, H. Ma and M. Lin, *Mater. Sci. Eng., C*, 2017, **76**, 139–143.
2 L. Cui, J. Wu, J. Li, Y. Ge and H. Ju, *Biosens. Bioelectron.*, 2014, **55**, 272–277.
3 H. Aydın, Y. Bulut and Ç. Yerlikaya, *J. Environ. Manage.*, 2008, **87**, 37–45.
4 P. S. Donnelly, Z. Xiao and A. G. Wedd, *Curr. Opin. Chem. Biol.*, 2007, **11**, 128–133.
5 R. Jiang, L. Chen, X. Bai, J. Ye, Y. Luo, L. Wang, C. Fan, H. Li, Y. Shi and Y. Xu, *Electroanalysis*, 2021, 0034.
6 X. Fang, X. Chen, Y. Liu, Q. Li, Z. Zeng, T. Maiyalagan and S. Mao, *ACS Appl. Nano Mater.*, 2019, **2**, 2367–2376.
7 Y. Ma, Y. Wang, D. Xie, Y. Gu, X. Zhu, H. Zhang, G. Wang, Y. Zhang and H. Zhao, *Chem. Eng. J.*, 2018, **347**, 953–962.
8 M. Yang, P. H. Li, S. H. Chen, X. Y. Xiao, X. H. Tang, C. H. Lin, X. J. Huang and W. Q. Liu, *Small*, 2020, **16**, 2070140.
9 J. Pang, H. Fu, W. Kong, R. Jiang, J. Y. Luo, Z. Zhao, J. Hou, K. Sun, Y. Zheng and L. Chen, *Chem. Eng. J.*, 2021, 133854.
10 Z.-G. Liu, X. Chen, J.-H. Liu and X.-J. Huang, *Electrochem. Commun.*, 2013, **30**, 59–62.
11 B. Cheng, L. Zhou, L. Lu, J. Liu, X. Dong, F. Xi and P. Chen, *Sensor. Actuator. B Chem.*, 2018, **259**, 364–371.
12 V. Y. Maldonado, P. J. Espinoza-Montero, C. A. Rusinek and G. M. Swain, *Anal. Chem.*, 2018, **90**, 6477–6485.
13 D. Sun and Z. Li, *J. Phys. Chem. C*, 2016, **120**, 19744–19750.
14 Q. Yang, Q. Xu and H.-L. Jiang, *Chem. Soc. Rev.*, 2017, **46**, 4774–4808.
15 X. Tu, Y. Xie, X. Ma, F. Gao, L. Gong, D. Wang, L. Lu, G. Liu, Y. Yu and X. Huang, *J. Electroanal. Chem.*, 2019, **848**, 113268.
16 Z. Lu, W. Zhao, L. Wu, J. He, W. Dai, C. Zhou, H. Du and J. Ye, *Sensor. Actuator. B Chem.*, 2021, **326**, 128957.
17 Z. Zeng, X. Fang, W. Miao, Y. Liu, T. Maiyalagan and S. Mao, *ACS Sens.*, 2019, **4**, 1934–1941.
18 D. Wang, Y. Ke, D. Guo, H. Guo, J. Chen and W. Weng, *Sensor. Actuator. B Chem.*, 2015, **216**, 504–510.
19 M. B. Poudel, G. P. Awasthi and H. J. Kim, *Chem. Eng. J.*, 2021, **417**, 129312.
20 X. Wang, Y. Qi, Y. Shen, Y. Yuan, L. Zhang, C. Zhang and Y. Sun, *Sensor. Actuator. B Chem.*, 2020, **310**, 127756.
21 Y. Zhang, H. Yu, T. Liu, W. Li, X. Hao, Q. Lu, X. Liang, F. Liu, F. Liu, C. Wang, C. Yang, H. Zhu and G. Lu, *Anal. Chim. Acta*, 2020, **1124**, 166–175.

22 J. Ru, X. Wang, X. Cui, F. Wang, H. Ji, X. Du and X. Lu, *Talanta*, 2021, **234**, 122679.
23 J. Zou, W. Qian, Y. Li, Q. Yu, Y. Yu, S. Chen, F. Qu, Y. Gao and L. Lu, *Appl. Surf. Sci.*, 2021, **569**, 150006.
24 X. Wang, Y. Xu, Y. Li, Y. Li, Z. Li, W. Zhang, X. Zou, J. Shi, X. Huang, C. Liu and W. Li, *Food Chem.*, 2021, **357**, 129762.
25 H. Hou, K. M. Zeinu, S. Gao, B. Liu, J. Yang and J. Hu, *Energy Environ. Mater.*, 2018, **1**, 113–131.
26 H. Qiu, M. Ye, Q. Zeng, W. Li, J. Fortner, L. Liu and L. Yang, *Chem. Eng. J.*, 2019, **360**, 621–630.
27 Y. Wang, L. Wang, W. Huang, T. Zhang, X. Hu, J. A. Perman and S. Ma, *J. Mater. Chem. A*, 2017, **5**, 8385–8393.
28 M. B. Poudel and H. J. Kim, *J. Energy Chem.*, 2022, **64**, 475–484.
29 G. P. Awasthi, S. P. Adhikari, S. Ko, H. J. Kim, C. H. Park and C. S. Kim, *J. Alloys Compd.*, 2016, **682**, 208–215.
30 G. P. Awasthi, M. B. Poudel, M. Shin, K. P. Sharma, H. J. Kim and C. Yu, *J. Energy Storage*, 2021, **42**, 208–215.
31 J. Yukird, P. Kongsittikul, J. Qin, O. Chailapakul and N. Rodthongkum, *Synth. Met.*, 2018, **245**, 251–259.
32 R. Karthik and S. Thambidurai, *J. Alloys Compd.*, 2017, **715**, 254–265.
33 J. Liu, G. Zhu, M. Chen, X. Ma and J. Yang, *Sensor. Actuator. B Chem.*, 2016, **234**, 84–91.
34 K. Y. Kumar, H. B. Muralidhara, Y. A. Nayaka, J. Balasubramanyam and H. Hanumanthappa, *Powder Technol.*, 2013, **239**, 208–216.
35 X. Wang, W. Cai, S. Liu, G. Wang, Z. Wu and H. Zhao, *Colloids Surf. A Physicochem. Eng. Asp.*, 2013, **422**, 199–205.
36 M. Bagheri, S. Azizian, B. Jaleh and A. Chehregani, *J. Ind. Eng. Chem.*, 2014, **20**, 2439–2446.
37 F. Ahmadijokani, H. Molavi, M. Rezakazemi, S. Tajahmadi, A. Bahi, F. Ko, T. M. Aminabhavi, J.-R. Li and M. Arjmand, *Prog. Mater. Sci.*, 2021, 100904.
38 L. Cui, J. Wu and H. Ju, *Biosens. Bioelectron.*, 2015, **63**, 276–286.
39 P. H. Li, Z. Y. Song, M. Yang, S. H. Chen, X. Y. Xiao, W. Duan, L. N. Li and X. J. Huang, *Anal. Chem.*, 2020, **92**, 16089–16096.
40 M. Ding, N. Yao, C. Wang, J. Huang, M. Shao, S. Zhang, P. Li, X. Deng and X. Xu, *Nanoscale Res. Lett.*, 2016, **11**, 205.
41 P. Wu, C. Liu, Y. Luo, K. Wu, J. Wu, X. Guo, J. Hou and Z. Liu, *Front. Mater. Sci.*, 2019, **13**, 43–53.
42 L. Shen, S. Liang, W. Wu, R. Liang and L. Wu, *J. Mater. Chem. A*, 2013, **1**, 11473–11482.
43 P. Tian, X. He, W. Li, L. Zhao, W. Fang, H. Chen, F. Zhang, W. Zhang and W. Wang, *J. Mater. Sci.*, 2018, **53**, 12016–12029.
44 J. Xu, S. He, H. Zhang, J. Huang, H. Lin, X. Wang and J. Long, *J. Mater. Chem. A*, 2015, **3**, 24261–24271.
45 C. Zhang, Z. Cao, G. Zhang, Y. Yan, X. Yang, J. Chang, Y. Song, Y. Jia, P. Pan, W. Mi, Z. Yang, J. Zhao and J. Wei, *Microchem. J.*, 2020, 158.
46 X. Xie, D. Stüben, Z. Berner, J. Albers, R. Hintsche and E. Jantzen, *Sensor. Actuator. B Chem.*, 2004, **97**, 168–173.
47 H. Shi, F. Zhu, X. Zhou, H. Li, F. Yang, X. Zhang and J. Liu, *J. Electroanal. Chem.*, 2019, **840**, 328–337.

48 C. Guo, C. Wang, H. Sun, D. Dai and H. Gao, *RSC Adv.*, 2021, **11**, 29590–29597.

49 L. Ma, X. Zhang, M. Ikram, M. Ullah, H. Wu and K. Shi, *Chem. Eng. J.*, 2020, **395**, 125216.

50 M. Lu, Y. Deng, Y. Luo, J. Lv, T. Li, J. Xu, S.-W. Chen and J. Wang, *Anal. Chem.*, 2018, **91**, 888–895.

51 Z. Guo, D. D. Li, X. K. Luo, Y. H. Li, Q. N. Zhao, M. M. Li, Y. T. Zhao, T. S. Sun and C. Ma, *J. Colloid Interface Sci.*, 2017, **490**, 11–22.

52 T. Priya, N. Dhanalakshmi, V. Karthikeyan and N. Thinakaran, *J. Electroanal. Chem.*, 2019, **833**, 543–551.

53 S. Duan and Y. Huang, *J. Electroanal. Chem.*, 2017, **807**, 253–260.

54 X. Zhu, B. Liu, H. Hou, Z. Huang, K. M. Zeinu, L. Huang, X. Yuan, D. Guo, J. Hu and J. Yang, *Electrochim. Acta*, 2017, **248**, 46–57.

55 L. Yu, Q. Zhang, B. Yang, Q. Xu, Q. Xu and X. Hu, *Sensor. Actuator. B Chem.*, 2018, **259**, 540–551.

56 M. R. Awual, *Chem. Eng. J.*, 2016, **300**, 264–272.

57 C. Fan, X. Zhai, L. Chen, S. Peng, R. Jiang, J. Yu, Y. Li, Y. Zhang, W. Kong, G. Ge and X. Guo, *J. Mater. Chem. A*, 2021, **9**, 22277–22290.

58 W. Zhang, S. Fan, X. Li, S. Liu, D. Duan, L. Leng, C. Cui, Y. Zhang and L. Qu, *Mikrochim. Acta*, 2019, **187**, 69.